Effect of cathode porosity on the Lithium air cell oxygen reduction reaction – a rotating ring-disk electrode investigation

Jeongwook Seo[a,*,#] Shrihari Sankarasubramanian[a,*,#,1], Nikhilendra Singh[b], Fuminori

Mizuno[b,c], Kensuke Takechi[b], and Jai Prakash[a,*]

[a] Center for Electrochemical Science and Engineering, Department of Chemical and Biological Engineering, Illinois Institute of Technology, 10 West 33rd Street, Chicago, IL 60616, USA

[b] Toyota Research Institute of North America, 1555 Woodridge Avenue, Ann Arbor, Michigan 48105, USA

Abstract

The kinetics of the oxygen reduction reaction (ORR) on the practical air cathode in a Lithium air cell, which is conventionally composed of porous carbon with or without catalysts supported on it, was investigated. The mechanism and kinetics of the oxygen reduction reaction (ORR) was studied on a porous carbon electrode in an oxygen saturated solution of 0.1M Lithium bis-trifluoromethanesulfonimidate (LiTFSI) in Dimethoxyethane (DME) using cyclic voltammetery (CV) and the rotating ring-disk electrode (RRDE) technique. The oxygen reduction and evolution reactions were found to occur at similar potentials to those observed on a smooth, planar glassy carbon (GC) electrode. The effect of the porosity and the resultant increase in surface area were readily observed in the increase in the transient time required for the intermediates to reach the ring and the much larger disk currents (compared to smooth, planar GC) recorded respectively. The RRDE data was analyzed using a kinetic model previously developed by us and the rate constant of the elementary reactions calculated. The rates constant for the electrochemical

---

[*] To whom correspondence may be addressed: E-mail address: jseo16@hawk.iit.edu (J.Seo), ssanka11@hawk.iit.edu (S, Sankarasubramanian), prakash@iit.edu (J.Prakash)

[#] These authors contributed equally to this work.

[c] Present address: Battery Material Engineering & Research Division, Toyota Motor Corporation, Higashifuji Technical Center, 1200, Mishuku, Susono, Shizuoka, 410-1193 Japan

[1] Present address: Department of Energy, Environmental and Chemical Engineering, Washington University in St. Louis, 1 Brookings Dr, St. Louis, MO 63130, USA

reactions were found to be similar in magnitude to the rate constants calculated for smooth GC disks. The porosity of the electrode was found to decrease the rate of desorption of the intermediate and the product and delay their diffusion by shifting it from a Fickian regime in the electrolyte bulk to the Knudsen regime in the film pores. Thus, it is shown that the effect of the electrode porosity on the kinetics of the ORR is physical rather than electrochemical.

Keywords: Oxygen Reduction Reaction, Lithium-oxygen battery, electrochemical kinetics, carbon electrode, rotating ring-disk electrode.

1. Introduction

The mitigation of "range anxiety" hindering the adoption of electric vehicles (EV) requires that EVs on a single charge match the range of a gasoline powered car with a full tank. A range of 500 miles/charge, which would satisfy this requirement, requires the commercialization of "beyond Li-ion" battery systems. The Li-O_2 cell is one of the best candidates due to its high theoretical specific energy of 3505 Wh Kg^{-1} which is significantly higher than current lithium-ion cells [1,2]. The practical use of this promising technology is beset by problems of the high overvoltage leading to low columbic efficiency and low power density [1-3], Li dendrite growth on the anode [4], side reactions with N_2 and H_2O in air [5,6], and unstable electrolytes leading to short cycle life [7-10],

During oxygen reduction reaction (ORR), O_2 or O_2^- formed by outer sphere electron transfer, is adsorbed onto the cathode and reacts with Li$^+$ to form LiO$_2$ though net one electron transfer. Li$_2$O$_2$ is formed from LiO$_2$ via a subsequent electrochemical reaction or by chemical disproportionation reaction [10, 11]. An examination of the literature indicates that the two-electron transfer reaction has not been reported. A consensus exists in the literature that Li$_2$O$_2$ is

the final discharge product of the Li-O₂ cell following extensively studies using in-situ [12-14] and ex-situ techniques [15] but the elementary steps involved in the ORR are less well understood. The net one electron transfer observed herein has led to the chemical disproportionation of LiO_2 being considered the major reaction route [14-19] with reports of its occurrence in the electrolyte bulk [15-17], on the electrode surface [18,19] or as a hybrid surface-electrolyte mechanism [14]. It is evident from the literature that analyses of data from the same technique such as SERS [12,38], AFM [34,40] or EQCM [19,34] for example, have led to radically different conclusions as to the overall mechanism. Several of these studies [12,34,40] also employ unstable [11,41,42] DMSO as the electrolyte solvent, necessitating the data obtained to be examined in this context. Thus, the elucidation of the Li-O2 ORR mechanism is complicated by the interplay of factors such the solvent [15,16,21], salt [43,44], applied overpotential [14] and electrolyte water content [6,21].

The applicability of the rotating ring-disk electrode (RRDE) technique has been reported previously [11, 21, 22, 35] to elucidate complex reaction mechanisms in non-aqueous systems. The present study seeks to use the RRDE technique to examine the Li^+ ORR on practical, porous carbon electrodes. Porous carbon electrodes have been extensively used as cathodes for Li-air cells [3,4,10,22-27]. The influence of the carbon surface on Li_2O_2 deposits on the cathode has bene examined by us previously [23] and others have examined the corresponding oxygen evolution reaction (OER) [25]. In the present study, we combine RRDE measurements and a kinetic model to calculate the rate constants for each of the elementary steps and the competition between the surface and bulk reactions is quantified.

2. Experimental Methods

The carbon black mixture was prepared by mixing 10 mg Carbon black (CB, acetylene, 100% compressed, surface area: 80 m^2g^{-1}, >99.9 %, Alfa Aesar) with 10 wt% polytetrafluorethylene solution (PTFE, 60 wt% dispersion in water, Sigma Aldrich) followed by addition of 3 ml isopropanol to the CB/PTFE mixture solution to dilute the mixture. The mixture was dispersed with a sonicator (Qsonica, frequency: 20 KHz) for 10 minutes at room temperature. The glassy carbon (GC) disk of the RRDE system was roughened using sand paper and recessed ~ 1 mm below the lip of the surrounding teflon holder. The CB film was deposited by dropping 7 μl CB/PTFE slurry onto the recessed, roughened GC disk electrode (surface area: 0.196 cm^2) and dried in an oven at 40 ˚C for 15 minutes. This CB coating process was repeated three times until it uniform surface coverage was achieved and the film was flush with the RRDE assembly surface. Finally, the porous CB disk electrode was dried in a vacuum oven at 40 ˚C for 12 hours to remove all water and solvent.

The 0.1M solution of Lithium bis-trifluoromethanesulfonimidate (LiTFSI) (99.95%, Aldrich) in 1,2-Dimethoxyethane (DME) (Sigma-Aldrich, ReagentPlus, ≥99%) was prepared in a MBraun argon filled glove box with H_2O and O_2 levels <0.5ppm. The LiTFSI salt was dried in a vacuum oven for 24 hours at 40˚C and DME was distilled, argon purged and stored in an argon filled glove box to ensure absence of moisture before use. The water content in the "as-received" DME was measured using Karl-Fisher titration (Mettler Toledo C30 Coulometric KF Titrator) and the water content was found to be 77.6 ppm. Similarly, the water content of the electrolyte was measured after preparation and found to be 76.8 ppm.

The electrochemical experiments were carried out with a multi-channel potentiostat (Solartron Analytical) with independent leads for potential and current. A 50-ml flask was used for the RRDE measurement with a custom designed Teflon top with four openings for working,

reference, counter electrode and the gas purge line respectively. The three-electrode system consisted of Pt gauze (Alfa Aesar, 45 mesh, <99.9%) on a Pt wire as reference and counter electrode. The working electrode was a Pine instruments RRDE with the CB coated GC disk surrounded by a Pt ring with a rated collection efficiency (N) of 0.25 and used in conjunction with the supplied rotor shaft and gas purged bearing assembly. The entire setup was assembled in the glove box and sealed. Upon transfer out of the glovebox, the gas inlet was immediately connected to an Ar source to maintain the Ar blanket over the electrolyte surface. The gas purged bearing assembly was connected to a second Ar source to prevent ingress of atmospheric air during RRDE shaft rotation. The Pt pseudo-reference was calibrated with respect to the Li/Li^+ couple using a ferrocene/ferrocenium (Fc/Fc^+) internal reference as recommended by IUPAC [45]. The calibration procedure and resultant graphs are in supplementary materials section 1.

The background cyclic voltammograms (CV) were measured in Ar saturated state after a 30 min Ar purge. The CVs were then measured using different scan rates in the O_2 saturated condition after O_2 purge for 1 hour. For the RRDE measurements, the working electrode rotation rate was controlled by a MSRX speed control (Pine Instrument). The ring potential was held at 3.08 V which was chosen to achieve complete oxidation of reduced species produced at the disk. The linear sweep voltammograms (LSVs) were measured from 2.2 to 1.0 V vs Li/Li^+ based on the location of the ORR peak identified from the CV.

3. Results and discussions

3.1 Electrochemical measurements

The oxygen reduction and oxygen evolution current was measured on the porous CB coated GC electrode disk. Figure 1 shows CVs performed over the potential range of the ORR and OER

with different scan rates in O_2 saturated 0.1 M LiTFSI in DME electrolyte. The background CV was measured in Ar saturated electrolyte and parasitic side reactions were not observed in this voltage range. A peak seperation of 1300 mV was measured with 5 mV.s^{-1} scan rate and hence was found to be higher than the theoretical value for a one electron reversible reaction (59 mV). The ORR and OER peak shifts were seen to be in agreement with the suggestion of a 30/α mV shift for a 10 fold increase in scan rate [29].

The electrochemical kinetic analysis for ORR was carried by combining the RRDE technique with an electro-kinetic model. A detailed discussion of the use of RRDE measurements for non-aqueous ORR reactions can be found in our recent works [11, 20]. Figure 2 shows the RRDE measurements on the porous CB disk and Pt ring system carried out at a scan rate of 2 mV.s^{-1}. The LSVs of porous CB disk showed the typical observation that the limiting currents (i_L) is directly proportional to the square root of rotation rate ($\omega^{-\frac{1}{2}}$).

3.2 Kinetic analysis

The Koutecky-Levich equation describes the current measured by a RRDE if the ORR kinetics is first order with respect to dissolved oxygen and the disk current and square root of rotation rate have the relation given by equation (1):

$$\frac{1}{i} = \frac{1}{i_k} + \frac{1}{i_L} = \frac{1}{i_k} + \frac{1}{B\sqrt{\omega}}$$

(1)

where i$_k$ is the kinetic current. Thus, the slope of a typical Koutecky-Levich (K-L) plot (i^{-1}vs. $\omega^{-\frac{1}{2}}$) as shown in Figure 3 would equal a constant B given by equation (2):

$$B = 0.62\, nFAD^{\frac{2}{3}}v^{-\frac{1}{6}}C_b$$

(2)

Where F is 96,485 C mol^{-1}, A is the geometric area of disk, D is the diffusion coefficient of O$_2$ (2.78 x 10^{-6} cm^{2}s^{-1} in 0.1M LITFSI/DME) [22], Cb is the bulk concentration of O$_2$ (9.57 x 10-6 mol/cm^3) [30], ν is kinematic viscosity (5.22 x 10^{-3} cm s^{-1}) that was measured using a Ubbelohde viscometer. The presence of the CB film potentially complicates the analysis of the K-L plot compared to the case of the smooth electrode described above. In case the film was porous enough to allow for flow inside the pores, the current versus rotation rate profile has been shown to have a sigmoidal profile with the current being linear below a certain critical rotation rate and increasing exponentially above this value [33]. On the other hand, for dense porous materials like most carbons used in electrodes, the pores would be too small for flow to occur inside them [33]. The transport regime in the film in such cases is expected to be dominated by diffusion, with the contributions from Fickian and Knudsen diffusion depending on the pore size distribution. Apart from the convective transport to the disk surface and kinetics on the disk surface that can serve as the limiting factor (depending on the potential), in a porous electrode system we may also need to consider the diffusive transport through the film, possible reaction rate limitation at the redox centers inside the film and partitioning between the film surface and the film bulk (i.e. inside the pores) [29]. The various possibilities and the Koutecky-Levich like equations applicable to these cases are comprehensively discussed elsewhere [29,36]. It is to be noted that the effect of these various possible limiting factors is typically an additional contribution to the limiting current leading to a non-zero intercept for the $1/i$ vs. $\omega^{-\frac{1}{2}}$ plots at the limiting current region. Depending on the film and the postulated limiting factor in the film, this non-zero intercept is treated suitably. The slope of the K-L plot and hence kinetic calculations such as the number of electrons is unaffected. In the present case, for a uniform, conducting carbon film whose thickness is an order of magnitude less than its diameter, the diffusion process in the film is believed to be dominant

contribution to the film current. To account for this film current, we may re-write the K-L equation as follows [29]:

$$\frac{1}{i} = \frac{1}{i_k} + \left[\frac{1}{i_{Levich}} + \frac{1}{i_{film}} \right]$$ (3)

The depletion layer at the disk disappears at high enough rotation rate and hence we may assume that the reactant concentration exposed to the disk would be the same as the bulk concentration. Thus, the film current maybe represented as [29]:

$$i_{film} = \frac{nFAD_{film}\kappa C_{O_2,bulk}}{\phi}$$ (4)

The reaction occurring on the film surface vs. the pores can be distinguished through the partition coefficient κ (assuming the same rate expression in both the pores and the surface) and the pore diffusion (possibly Fickian) can be characterized by the film diffusion coefficient D_{film}. Interestingly, it was observed that while there is a small film current at the start of the limiting current region (1.8V), this current disappears at higher overpotentials (1.4V). This may indicate that at high enough overpotentials the reactions on the surface are so rapid as to consume all reactants reaching the surface before they have an opportunity to diffuse into the film bulk. Nevertheless, calculating the $\frac{D_{film}\kappa}{\phi}$ term using the film current at 1.8V (1.03mA), a value of 5.7 x 10^{-5} m.s^{-1} was obtained. Since the film is ~1mm thick, this leads to a film diffusion coefficient of 5.7 x 10^{-8} m^2. s^{-1}. This is two orders of magnitude lower than the bulk diffusion coefficient of oxygen (2.78 x 10^{-6} cm^{2}s^{-1} in 0.1M LITFSI/DME).

Alternatively, the contribution of film diffusion can be evaluated using the disk to ring transient time. The transient time is related to the reactant diffusion coefficient as follows [37]:

$$T_s = K \left(\frac{\nu}{D_{O_{2,bulk}}} \right)^{\frac{1}{3}} \omega^{-1} \qquad (5)$$

K is a RRDE geometry dependent proportionality factor given by $K = 43.12 \left(\log \left(\frac{r_2}{r_1} \right) \right)^{\frac{2}{3}}$. In the present case, it is 10.1 rpm.s, leading to a calculated value of the transient time at 400 rpm of 0.3s. Whereas experimentally, we observe a transient time of ~14s. While there may be a contribution from the difference between the calculated and actual K values (due to variations in RRDE geometry) these would not be sufficient to explain the two orders of magnitude variation (the experimentally determined value of K in reference 37 was 11). But since the film and bulk diffusion coefficients vary by two orders of magnitude, the possible reason for this discrepancy is apparent. The slow product diffusion through the film on the disk, slows down its detection at the ring. Thus, analysis of both the reaction currents at the disk and product oxidation currents at the ring show that transport through the film plays a major role in the determining reaction site (film surface vs. film pores) and rate of product transport through the film (Li_2O_2 precipitation vs. pore clogging). This is a vital first step in understanding the Li^+ ORR in practical electrodes.

The plots from the mixed control region between 1.5 V to 1.7 V were used to calculate the total number of electrons transferred in the reaction and this was found to equal 1.07 within 10% error. This calculation was carried out using the geometric surface area of the electrode. The actual surface area measured by techniques such as N_2 adsorption (BET) is not applicable herein as the electroactive surface area is not necessarily the same as the physical surface area. The variation of ORR kinetics by adsorption site has been discussed by us elsewhere [20]. Further, the bulk diffusion coefficient of oxygen is used as the effective diffusion coefficient.

The combination of the total number of electrons with the information on the rate determining step obtained from a Tafel plot allowed us to describe the overall electrochemistry of

the present system. Semilog plots of kinetic current and the disk potential (Tafel plot) are depicted in the Figure 4. The kinetic current and the overpotential is related by the Tafel equation:

$$\eta = a + b.\log{(i_k)} \tag{6}$$

Where

$$a = \frac{2.3RT}{\alpha.F}.\log i_0 \tag{7}$$

$$b = -\frac{2.3RT}{\alpha.F} \tag{8}$$

The kinetic current i_k is determined by a rearrangement of the Koutecky-Levich equation ($i_k = i.i_L/(i_L - i)$) to obtain a relationship between the disk current and the limiting current. The slope of this plot indicates the rate determining step. In the present case, a value of 390 mV.dec^{-1} was obtained which was found to be at odds with the theoretical value (118 mV.dec^{-1} with transfer coefficient (α) = 0.5) for the first electron transfer step being rate determining. This anomalous value of the Tafel slope points to deviation in the value of the transfer coefficient from the conventional value of 0.5 to 0.16 as described by us previously [22]. This indicates an asymmetric energy landscape for the anodic and cathodic directions of the cathode reactions caused by the solvent interactions has been described by us elsewhere [22].

To calculate the individual reaction rate constants for the elementary steps multiple possible Li-O$_2$ ORR pathways depicted in the Figure 5 were considered. The initial step consists of the adsorption of O$_2$ on the cathode surface and subsequent production of LiO$_2$. Following the production of LiO$_2$, various possible reduction pathways were considered – further electrochemical reduction to produce Li$_2$O$_2$, chemical disproportionation reaction on the surface between adjacent LiO$_2$ to produce Li$_2$O$_2$ and desorption followed by chemical disproportionation

to produce Li_2O_2 in the electrolyte bulk. However, the four-electron reaction to produce Li_2O was not considered in this reaction scheme due to lack of experimental reports of Li_2O as the reduction product. The effect of water on the reaction was a key consideration. It has been reported that the surface or the solution phase reaction dominates based on the water content [46]. The present model considers both surface and solution mechanisms and hence this variability is implicitly accounted for. Further, the amount of water is in between the limits for transition between a largely surface based (<30ppm) to a largely solution based mechanism (> ~2000ppm). Hence a model based on competitive solution and surface based mechanisms would be most representative of the present system. Efforts to explicitly incorporate side reactions with water, its possible catalytic activity and its effects on the nucleation of Li_2O_2 are ongoing.

The reactions were described by typical kinetic equations along with equations for the disk and ring currents. The equations are as follows:

$$k_1[O_{2(a)}] = (k_3 + k_4 + k_5)[LiO_{2(a)}] \tag{9}$$

$$k_5[LiO_{2(a)}] - k_6[LiO_{2*}] = Z\omega^{\frac{1}{2}}[LiO_{2*}] \tag{10}$$

$$i_D = nFA\{(k_1 + 2k_2)[O_{2(a)}] + k_3[LiO_{2(a)}]\} \tag{11}$$

$$i_R = nFANZ\omega^{\frac{1}{2}}[LiO_{2*}] \tag{12}$$

Where Z is a mass transport relation given by:

$$Z = 0.62D^{\frac{2}{3}}\nu^{-\frac{1}{6}} \tag{13}$$

RRDE kinetics models from the literature for aqueous ORR [31, 32] and our prior work [11, 21, 22] were adapted to the present system to obtain the following relating the disk and ring current:

$$N\left(\frac{I_D}{I_R}\right) = \left(\frac{Ak_6}{k_5}\right)\left(\frac{1}{Z\omega^{\frac{1}{2}}}\right) + \left(\frac{A}{k_5}\right) \tag{14}$$

Where A is reaction rate constant relation given by:

$$A = 1 + \left(\frac{2k_2(k_3 + k_4 + k_5)}{k_1}\right) + k_3 \tag{15}$$

The kinetic relations were simplified based on our experimental observations. The Koutecky-Levich plots indicated that the overall reaction involved the transfer of a single electron. Thus, the direct two-electron and series based two-electron pathway to produce Li_2O_2 was eliminated ($k_2 = k_3 = 0$). The simplified model was further analyzed to obtain individual reaction rate constants.

Figure 6 shows the distribution of disk and ring current ($N(i_D/i_R)$ vs. square root of the rotation rate ($\omega^{-1/2}$). This plot is expected to yield straight lines with different slopes (S) and intercept (J) at different potentials based on the simplified form of equation (14) where A=1. The slopes (S) and intercepts (J) at different potentials from Figure 6 were plotted in the Figure 7. The slope and intercept are related by the following equation:

$$J = \left(\frac{Z}{k_6}\right) S \tag{16}$$

Figure 7 was seen to follow the prediction from the model that the intercept is zero and slope of the above plot allowed us to calculate the rate constant for the electrolyte bulk disproportionation reaction (k_6). The rate constant for desorption of LiO_2 from the surface (k_5) was then calculated from the slopes of the $N\left(\frac{i_D}{i_R}\right)$ plots. The value of k_5 was found to be smaller by three orders of magnitude as compared to the values the smooth, planar GC disk [22]. The rate of desorption was understood to be a function of the convective transport from the film surface reaction sites and diffusive (Fickian and/or Knudsen) transport from the intra-pore reaction sites. The material dependent intermediate binding energy could also play a role. The carbonaceous nature of the electrode in both the smooth and porous cases and the equal rates of rotation indicated that the variation in the desorption rates was a function of the porosity of the electrode. At the same

rotation rates (i.e. equal rates of convection), the smooth electrode would display purely Fickian diffusion whereas the porous electrodes can be expected to display a mixture of Fickian and Knudsen behavior (which is typically slower) depending on pore size distribution. Further, desorption would also depend on the species concentration gradient between the surface and the near surface electrolyte environment. This gradient could be non-uniform in highly tortuous electrodes and hence lead to non-uniform mass transport driving forces leading to a net slower rate of desorption. This was reflected in the large time transient between the observation of the mass transport limited current at the disk and the appearance of the corresponding current plateau at the ring.

The rate constant for the first electron transfer (k_1) was calculated from the rotation dependent relation between i_D, i_L described by equation (17) and depicted in Figure 8. The close match between the theoretical and experimental intercepts served as further validation of the present model.

$$\frac{i_L}{i_L - i_d} = 1 + \frac{k_1}{Z} \omega^{-\frac{1}{2}} \tag{17}$$

Having calculated k_1, k_5 and k_6, k_4 was calculated by rearranging equations (9)-(12) as follows:

$$k_4 = \frac{nFAZ_{O_2}\omega^{\frac{1}{2}}[O_{2(b)}]}{i_D}\left(\frac{k_1}{1+k_1}\right) - k_5 \tag{18}$$

The potential dependence of the various rate constants is summarized in Figure 9 and compared to the values for the smooth GC disk case from Sankarasubramanian et al. [22]. The potential dependent rate constant for the electrochemical one-electron transfer reaction (k_1) for both porous CB and smooth GC disk showed similar values as expected for chemically similar carbonaceous surfaces. This clearly indicated that any observed variation in the Li-O$_2$ cathode

reactions with changes in electrode porosity is physical in origin and not chemical. The rate constants for the chemical disproportionation reaction in the bulk (k_6) was found to be similar for both electrodes since the reactions in the electrolyte are independent of the physical or chemical properties of the electrode. The non-electrochemical steps - chemical disproportionation on the surface and desorption of LiO_2 and their associated rate constants k_4 and k_5 were found to display no potential dependence as expected. The value of k_4 was found to slightly increase with potential in the case of the porous CB disk. This was understood to occur due to a combination of the increasing production of LiO_2 at higher potentials and the hindered desorption of the LiO_2 due to the porous nature of the electrode and its associated transport limitations. The surface disproportionation reaction required the presence of two LiO_2 species in proximity and the occurrence of this increases with increasing concentration of the superoxide. While on the smooth electrode this increase in concentration can be expected to result in a proportionate increase in the rate of desorption, this was not understood to be the case on the porous electrode as the effective rate of pore and bulk transport was previously seen to be two orders of magnitude lower. Thus, the smooth GC electrode showed a slight decrease in the rate of surface disproportionation with potential while the porous electrode was found to display the opposite behavior.

Thus, the porous electrode increases the retention of the product species on the electrode and hence offers a possible avenue towards greater reversibility of Li_2O_2, with the trade-off being the overall slower rate of reaction due to the slowdown in the rate of the chemical disproportionation reaction on the surface. Further, the chemical disproportionation reaction is expected to dominate due to the transport properties of a porous electrode.

4. Conclusion

The present study examines the effect of porosity on the individual reactions comprising the ORR in Li-O_2 systems. Porous carbon was chosen as being representative of the typical electrode and catalyst support used in Li-O_2 cells. The porosity of the electrode was found to have a significant impact on the desorption of reaction intermediates and their further reaction on the surface while having minimal effect on the electrochemical reaction or chemical reactions in the electrolyte bulk. Porous electrodes offer a way to increase reversibility of the Li-O2 cell by minimizing loss of the Li_2O_2 product by precipitation but would also be hampered by increased passivation. The present study is expected to inform the choice of porous materials as non-aqueous cathodes and possibly influence the tailoring of optimum electrode porosity and tortuosity.

Acknowledgements

References:

1. Bruce P.G.; Freunberger S.A.; Hardwick L.J.; Tarascon J-M. Li–O_2 and Li–S batteries with high energy storage. *Nat. Mater.* **2011**, *11*, 19-29.

2. Christensen J.; Albertus P.; Sanchez-Carrera R.S.; Lohmann T.; Kozinsky B.; Liedtke R.; Ahmed J.; Kojic A. A Critical Review of Li/Air Batteries. *J. Electrochem. Soc.* **2012**, *159(2)*, R1-R30.

3. Lu Y-C.; Gasteiger H.A.; Crumlin E.; McGuire Jr. R.; Shao-Horn Y. Electrocatalytic Activity Studies of Select Metal Surfaces and Implications in Li-Air Batteries. *J. Electrochem. Soc.* **2010,** *157 (9)*, A1016-A1025.

4. Jung, H.G., Hassoun J., Park J.B., Sun, Y.K. Scrosati B., "An improved high-performance lithium-air battery." *Nat. Chem.,* **2012,** 4, 579–585.

5. Lim H-K.; Lim H.D.; Park K.Y.; Seo D.H.; Gwon H.; Hong J.; Goddard III W.A.; Kim H.; Kang K. Toward a Lithium–"Air" Battery: The Effect of CO_2 on the Chemistry of a Lithium–Oxygen Cell. *J. Am. Chem. Soc.* **2013,** *135(26)*, 9733-42.

6. Mizuno F.; Arthur T.S.; Takechi K. Water in Ionic Liquid for Electrochemical Li Cycling. *ACS Energy Lett.* **2016,** *1*, 542−547.

7. Assary R.S., Lau K.C., Amine K., Sun Y.K., Curtiss L.A., "Interactions of Dimethoxy Ethane with Li_2O_2 Clusters and Likely Decomposition Mechanisms for Li–O_2 Batterie." J. Phys. Chem. C, 117 (2013) 8041

8. Freunberger S. A., Chen Y., Peng Z., Griffin J. M., Hardwick L. J., Bardé F., Novák P., Bruce P.G., "Reactions in the Rechargeable Lithium–O_2 Battery with Alkyl Carbonate Electrolytes." J. Am. Chem. Soc., 133, (2011) 8040

9. Freunberger S.A., Chen Y., Drewett N.E., Hardwick L.J., Bardé F., Bruce P.G., "Oxygen Batteries "The Lithium–Oxygen Battery with Ether-Based Electrolytes." Angew. Chem., Int. Ed., 50, (2011) 8609-8613

10. Mizuno F., Nakanishi S., Kotani Y., Yokoishi S., Iba H., "Rechargeable Li-Air Batteries with Carbonate-Based Liquid Electrolytes." Electrochemistry, 78, (2010) 403

11. S. Sankarasubramanian, J. Seo, F. Mizuno, N. Singh, J. Prakash, "Rotating ring-disc electrode investigation of the aprotic superoxide radical electrochemistry on multi-crystalline surfaces

and correlation with Density functional theory modeling – implications for Lithium-air cells", J. Electrochem. Soc., 163(10), A2377-A2384 (2016).

12. Yu Q., Ye S., "In Situ Study of Oxygen Reduction in Dimethyl Sulfoxide (DMSO) Solution: A Fundamental Study for Development of the Lithium–Oxygen Battery." J. Phys. Chem. C, 119, (2015) 12236− 12250

13. Zhong L., Mitchell R.R., Liu Y., Gallant B.M., Thompson C.V., Huang J.Y., Mao S.X., Shao-Horn Y., "In Situ Transmission Electron Microscopy Observations of Electrochemical Oxidation of Li_2O_2." Nano Lett., 13, (2013) 2209−2214

14. Johnson L.; Li C.; Liu Z.; Chen Y.; Freunberger S.A.; Ashok P.C.; Praveen B.B.; Dholakia K.; Tarascon J-M.; Bruce P.G. The Role of LiO_2 Solubility in O_2 Reduction in Aprotic Solvents and its Consequences for LiO_2 batteries. *Nat. Chem.* **2014,** *6,* 1091-1099.

15. Laoire C.O.; Mukerjee S.; Abraham K.M.; Plichta E.J.; Hendrickson M.A. Influence of Nonaqueous Solvents on the Electrochemistry of Oxygen in the Rechargeable Lithium-Air Battery. *J. Phys. Chem. C* **2010,** *114,* 9178-9186.

16. Allen C.J.; Hwang J.; Kautz R.; Mukerjee S.; Plichta E.J.; Hendrickson M.A.; Abraham K.M. Oxygen Reduction Reactions in Ionic Liquids and the Formulation of a General ORR Mechanism for Li–Air Batteries. *J. Phys. Chem. C* **2012,** *116,* 20755-20764.

17. Trahan M.J.; Mukerjee S.; Plichta E.J.; Hendrickson M.A.; Abraham K.M. Studies of Li-Air Cells Utilizing Dimethyl Sulfoxide-Based Electrolyte. *J. Electrochem. Soc.* **2013,** *160(2),* A259-A267.

18. Viswanathan V.; Nørskov J.K.; Speidel A.; Scheffler R.; Gowda S.; Luntz A.C. Li−O_2 kinetic Overpotentials: Tafel Plots from Experiment and First- Principles Theory. *J. Phys. Chem. Lett.*

2013, *4,* 556-560.

19. McCloskey B.D.; Scheffler R.; Speidel A.; Girishkumar G.; Luntz A.C. On the mechanism of nonaqueous Li–O$_2$ electrochemistry on C and its kinetic overpotentials: some implications for Li–air batteries. *J. Phys. Chem. C* **2012,** *116,* 23897–23905.

20. S. Sankarasubramanian, N. Singh, F. Mizuno, J. Prakash, "Ab initio investigation of the Oxygen Reduction Reaction activity on noble metal (Pt, Au, Pd), Pt3M (M=Fe, Co, Ni, Cu) and Pd3M (M=Fe, Co, Ni, Cu) alloy surfaces, for Li-O$_2$ cells", J. Power Sources, 319, 202-209 (2016).

21. S. Sankarasubramanian, J. Seo, F. Mizuno, N. Singh, J. Prakash, "Enhancement of oxygen reduction reaction rate by addition of water to an oxidatively stable ionic liquid electrolyte for lithium-air cells", Electrochem. Commun., 73, 55-57 (2016).

22. S. Sankarasubramanian, J. Seo, F. Mizuno, N. Singh, J. Prakash, "Elucidating the Oxygen reduction reaction kinetics and the origins of the anomalous Tafel behavior at the Li-O$_2$ cell cathode", J. Phys. Chem. C, 121, 4789-4798 (2017).

23. Nakanishi S.; Mizuno F.; Nobuhara K.; Abe T.; Iba H. Influence of the carbon surface on cathode deposits in non-aqueous Li–O$_2$ batteries. *Carbon* **2012,** *50,* 4794-4803.

24. Yang Y., Sun Q., Li Y.S., Li H., Fu Z.W., "Nanostructured diamond like carbon thin film electrodes for lithium air batteries." J. Electrochem. Soc., 158, (2011) B1211–B1216

25. H. Beyer, S. Meini, N. Tsiouvaras, M. Piana, H.A. Gasteiger, "Thermal and electrochemical decomposition of lithium peroxide in non-catalyzed carbon cathodes for Li-air batteries", Phys. Chem. Chem. Phys., 15 (2013) 11025-11037.

26. A. Gueguen, P. Novak, and E.J. Berg, "XPS Study of the Interface Evolution of Carbonaceous Electrodes for Li-O_2 Batteries during the 1st Cycle", *J. Electrochem. Soc.*, **163** (13) A2545-A2550 (2016)

27. M. M. Ottakam Thotiyl, S.A. Freunberger, Z. Peng, and P.G. Bruce, "The Carbon Electrode in Nonaqueous Li−O_2 Cells", J. Am. Chem. Soc. 2013, 135, 494−500

28. M. M. Ottakam Thotiyl, S.A. Freunberger, Z. Peng, Y. Chen, Z. Liu and P.G. Bruce, "A stable cathode for the aprotic Li–O_2 battery", Nat. Mater., 12(11) (2013) 1050-1056.

29. Bard A.J.; Faulkner L.R. *Electrochemical Methods;* Wiley: New York, USA., 2001.

30. Sawyer D.T.; Chlerlcato Jr. G.; Angells C.T.; Nannl, Jr. E.J.; Tsuchiya T. Effects of Media and Electrode Materials on the Electrochemical Reduction of Dioxygen. *Anal. Chem.* **1982,** *54,* 1720–1724.

31. Wroblowa H.S.; Pan Y-C.; Razumney G. Electroreduction of oxygen: a new mechanistic criterion. *J. Electroanal. Chem.* **1976,** *69,* 195-201.

32. Hsueh K-L.; Chin D-T.; Srinivasan S. Electrode kinetics of oxygen reduction: A theoretical and experimental analysis of the Rotating ring-disk electrode method. *J. Electroanal. Chem.* **1983,** *153,* 79-95.

33. Bonnecaze R.T.; Mano N.; Nam B.; Heller A. On the Behavior of the Porous Rotating Disk Electrode. *J. Electrochem. Soc.,* **2007,** 154 (2), F44-F47.

34. Pozo M.D.; Torres W.R.; Herrera S.E.; Calvo E.J. New Evidence of LiO2 Dismutation in Lithium–Air Battery Cathodes. *ChemElectroChem* **2016**, 3, 1 − 5.

35. Torres W.; Mozhzhukhina N.; Tesio A.Y.; Calvo E.J. A Rotating Ring Disk Electrode Study of the Oxygen Reduction Reaction in Lithium Containing Dimethyl Sulfoxide Electrolyte: Role of Superoxide. *J. Electrochem. Soc.,* **2014,** 161 (14), A2204-A2209.

36. Leddy J.; Bard A.J.; Maloy J.T.; Saveant J.M. Kinetics of film-coated electrodes: Effect of a finite mass transfer rate of substrate across the film—solution interface at steady state. *J. Electroanal. Chem.,* **1985**, 187, 205-227.

37. Herranz J.; Garsuch A.; Gasteiger H.A. Using Rotating Ring Disc Electrode Voltammetry to Quantify the Superoxide Radical Stability of Aprotic Li−Air Battery Electrolytes. *J. Phys. Chem. C.* **2012,** 116, 19084−19094.

38. Zhai D.; Wang H-H; Yang J.; Lau K.C.; Li K.; Amine K.; Curtiss L.A. Disproportionation in Li−O_2 Batteries Based on a Large Surface Area Carbon Cathode. *J. Am. Chem. Soc.* **2013**, 135, 15364−15372.

39. Peng Z.; Freunberger S.A.; Hardwick L.J.; Chen Y.; Giordani V.; Barde F.; Novak P.; Graham D.; Tarascon J-M.; Bruce P.G. Oxygen Reactions in a Non-Aqueous Li^+ Electrolyte. *Angew. Chem. Int. Ed.* **2011,** 50, 6351 –6355.

40. Liu C.; Ye S. In Situ Atomic Force Microscopy (AFM) Study of Oxygen Reduction Reaction on a Gold Electrode Surface in a Dimethyl Sulfoxide (DMSO)-Based Electrolyte Solution. DOI: 10.1021/acs.jpcc.6b08718.

41. Sharon D.; Afri M.; Noked M.; Garsuch A.; Frimer A.A.; Aurbach D. Oxidation of Dimethyl Sulfoxide Solutions by Electrochemical Reduction of Oxygen. *J. Phys. Chem. Lett.* **2013,** 4, 3115−3119.

42. Kwabi D.G.; Batcho T.P.; Amanchukwu C.V.; Ortiz-Vitoriano N.; Hammond P.; Thompson C.V.; Shao-Horn Y. Chemical Instability of Dimethyl Sulfoxide in Lithium−Air Batteries. *J. Phys. Chem. Lett.* **2014,** 5, 2850−2856.

43. Gunasekara I.; Mukerjee S.; Plichta E.J.; Hendrickson M.A.; Abrahama K.M. A Study of the Influence of Lithium Salt Anions on Oxygen Reduction Reactions in Li-Air Batteries. *J. Electrochem. Soc.* **2015,** 162, A1055-A1066.

44. Burke C.M.; Pande V.; Khetan A.; Viswanathan V.; McCloskey B.D. Enhancing electrochemical intermediate solvation through electrolyte anion selection to increase nonaqueous Li–O2 battery capacity. *Proc. Natl. Acad. Sci. USA* **2015,** *112,* 9293-9298.

45. Gritzner G.; Kuta J.; Recommendations on reporting electrode potentials in nonaqueous solvents. *Pure & Appl. Chem.,* **1984,** *56 (4),* 461-466.

46. Aetukuri N.B.; McCloskey B.D.; García J.M.; Krupp L.E.; Viswanathan V.; Luntz A.C.; Solvating additives drive solution-mediated electrochemistry and enhance toroid growth in non-aqueous Li–O2 batteries. *Nat. Chem.,* **2015,** *7,* 50-56.

Figures and Tables
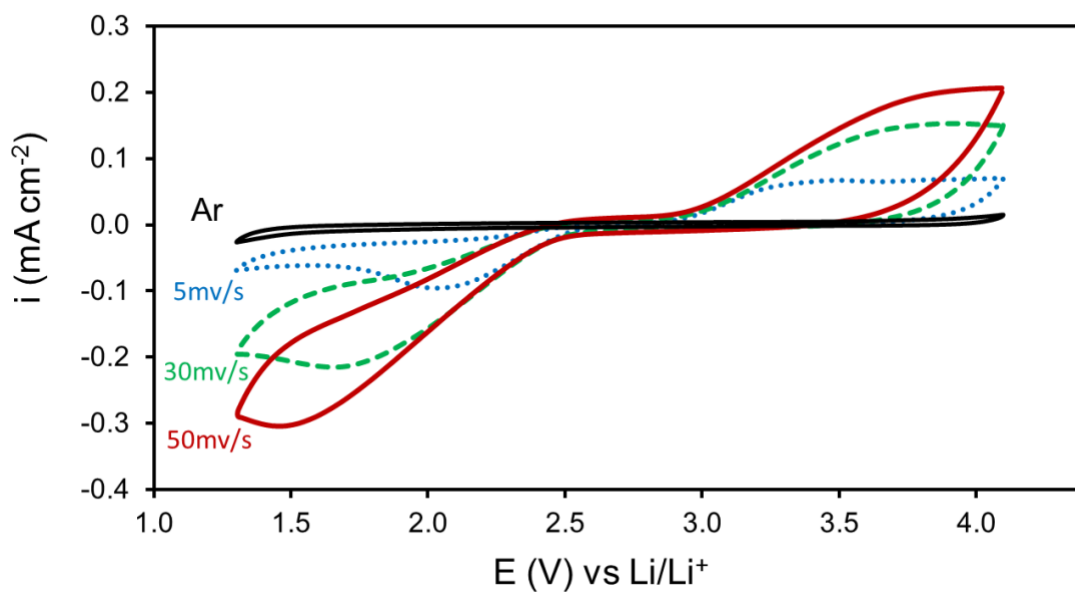
Figure 1. Cyclic voltammograms on a 1mm carbon black film (10% PTFE) deposited on a 0.196cm^2, roughened glassy carbon (GC) disk electrode in Ar and O$_2$ saturated 0.1 M LiTFSI in DME with varying scan rate.
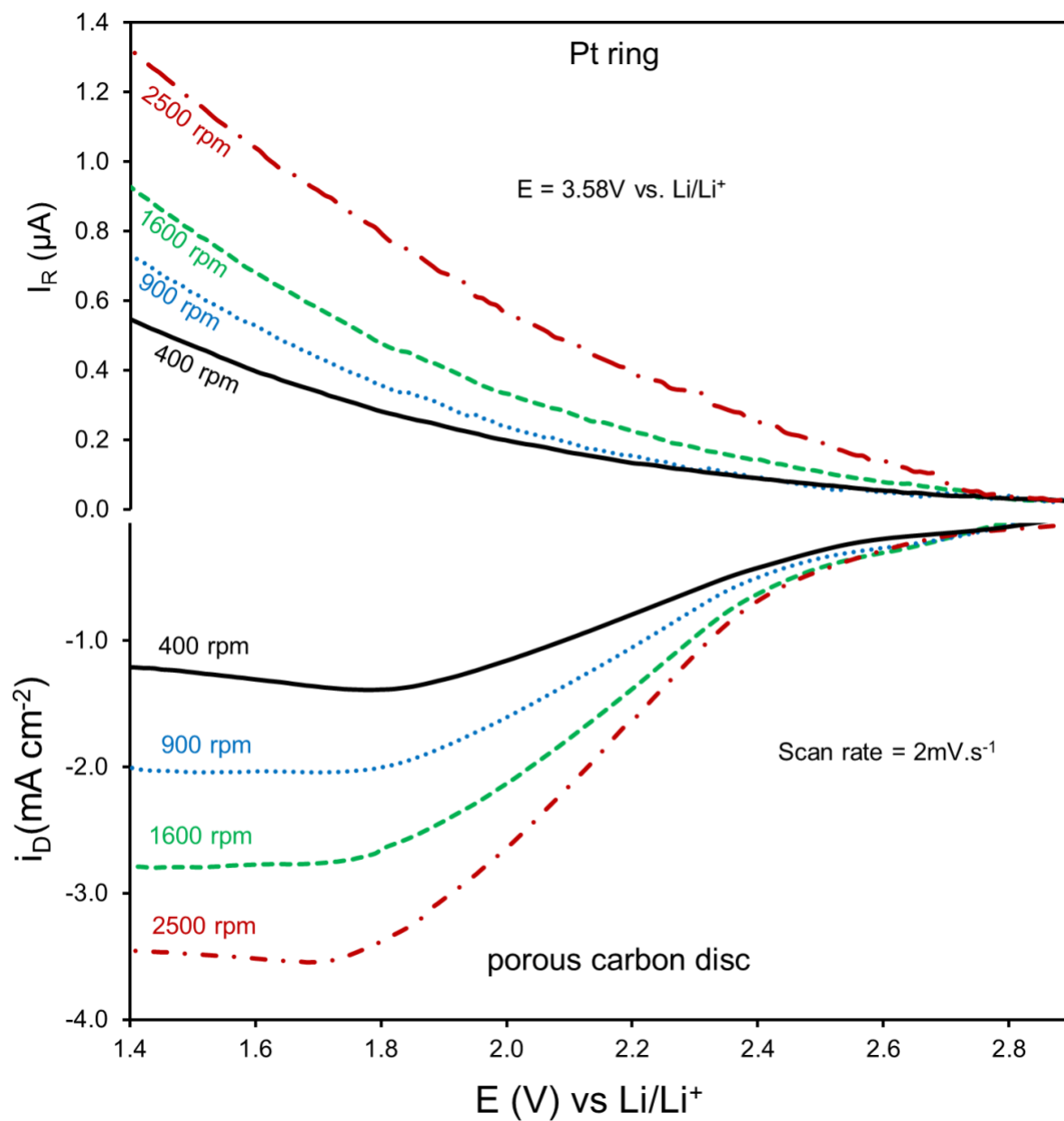
Figure 2. Linear sweep voltammograms on a rotating ring-disk electrode with a 1mm carbon black film (10% PTFE) deposited on a 0.196cm^2, roughened glassy carbon (GC) disk and platinum ring in O$_2$ saturated electrolyte. Disk currents were recorded at a scan rate of 2mVs^{-1}. Ring currents recorded with the Pt ring held at 3.08V vs Li/Li$^+$.
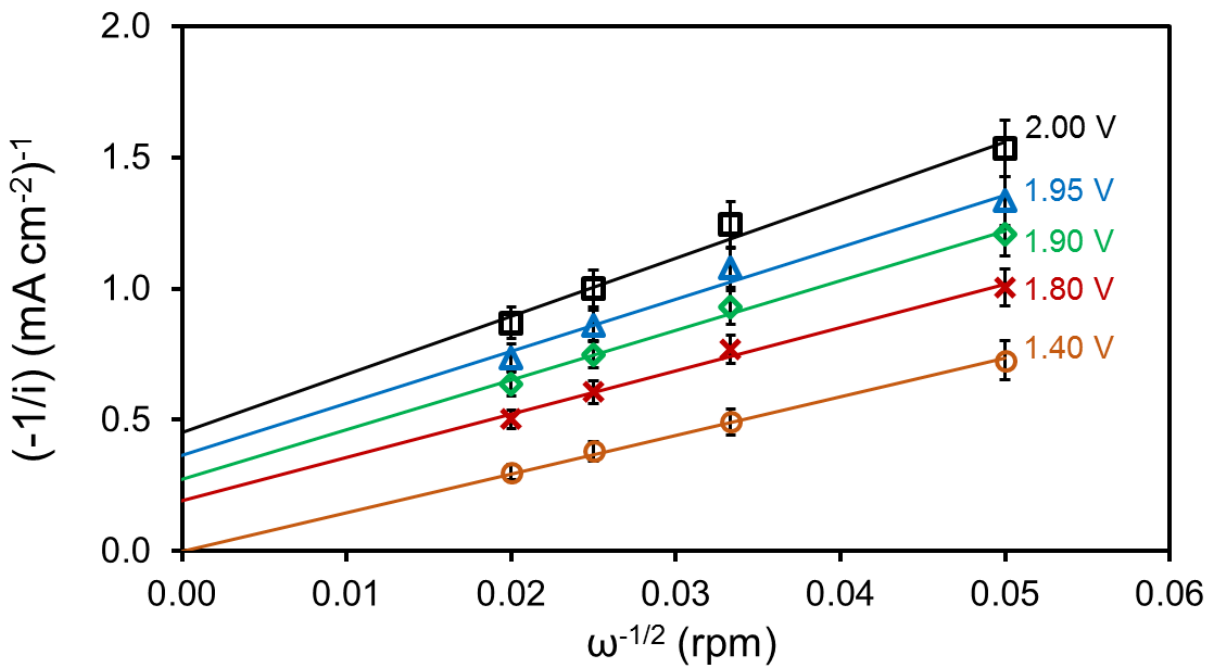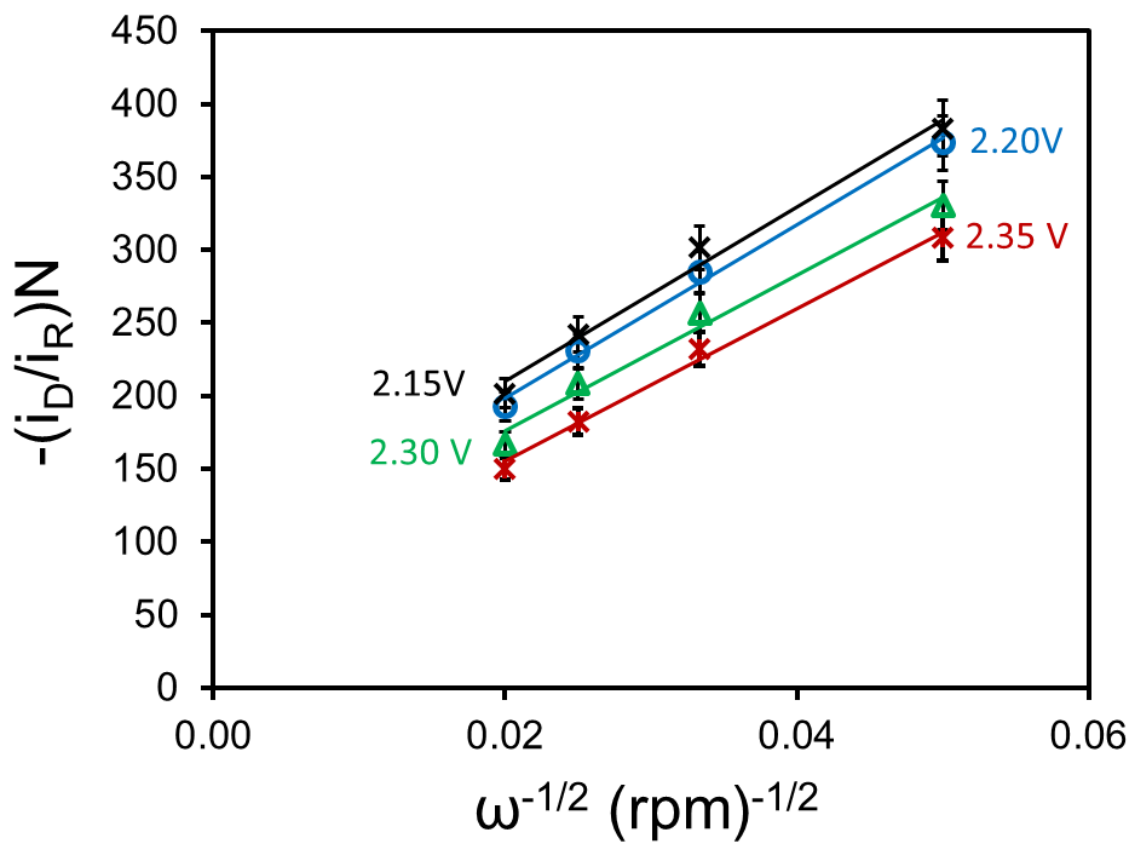
Figure 3. Koutecky-Levich ($-i^{-1}$ vs $\omega^{-1/2}$) plot for ORR on a 1mm carbon black film (10% PTFE) deposited on a 0.196cm^2, roughened glassy carbon (GC) disk electrode in 0.1M LiTFSI/DME electrolyte. Error bars depict 10% standard error.
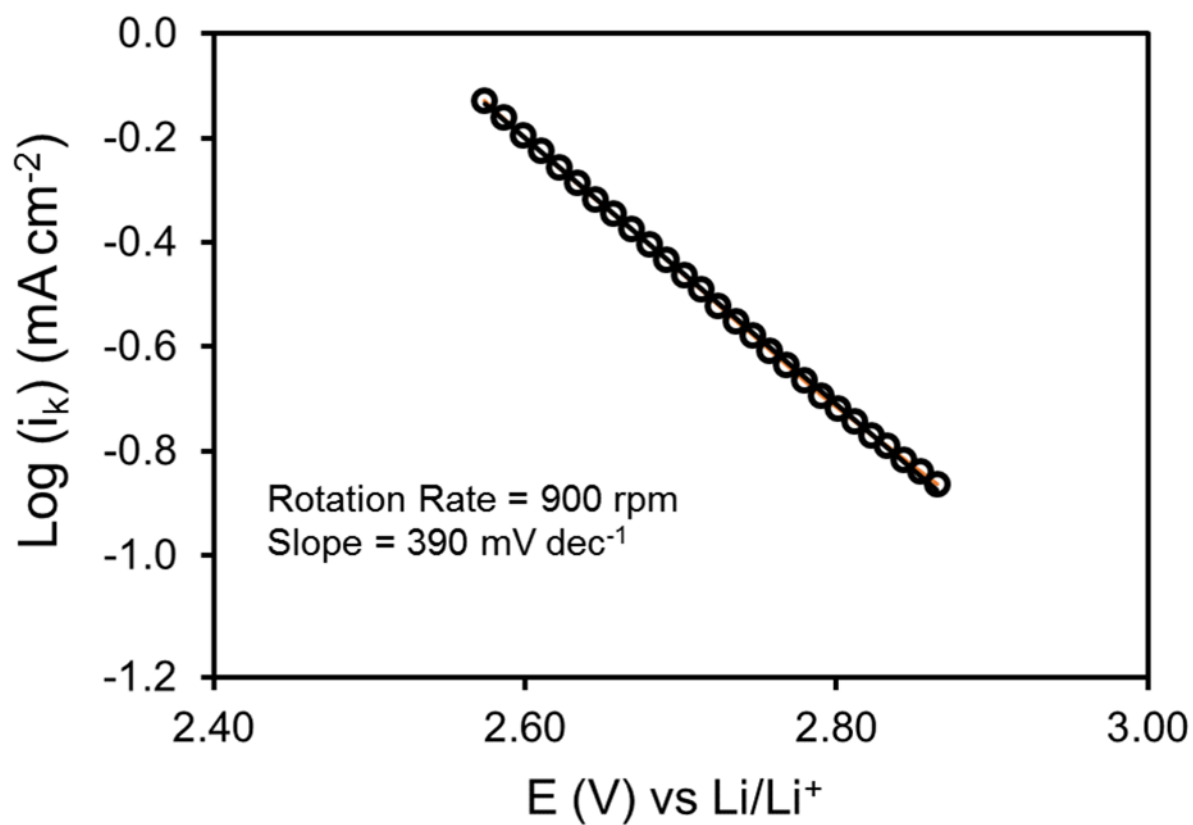
Figure 4. Tafel (log (i_k) vs E (V)) plot for ORR on a 1mm carbon black film (10% PTFE) deposited on a $0.196cm^2$, roughened glassy carbon (GC) disk electrode in 0.1M LiTFSI/DME electrolyte.
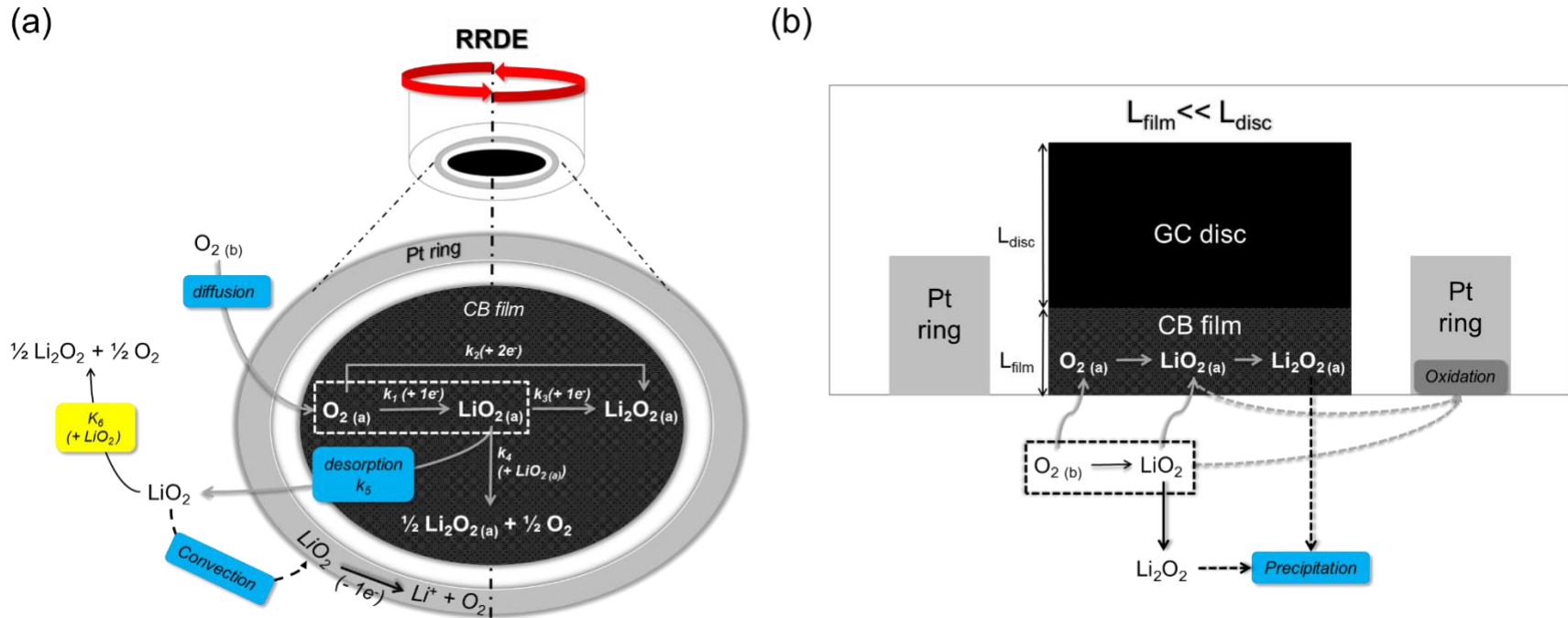
Figure 5. (a) Reaction scheme for the Oxygen reduction reaction on a Li-O₂ cell cathode and the kinetic model used with a Rotating ring-disk electrode (RRDE); (b) Cross-section view of the porous carbon black (CB) film disk electrode and the reactions therein (the reactions are illustrative and non-stoichiometric).

Figure 6. N(i_D/i_R) vs $\omega^{-1/2}$ plots for ORR on a 1mm carbon black film (10% PTFE) deposited on a 0.196cm^2, roughened glassy carbon (GC) disk electrode in 0.1M LiTFSI/DME electrolyte.
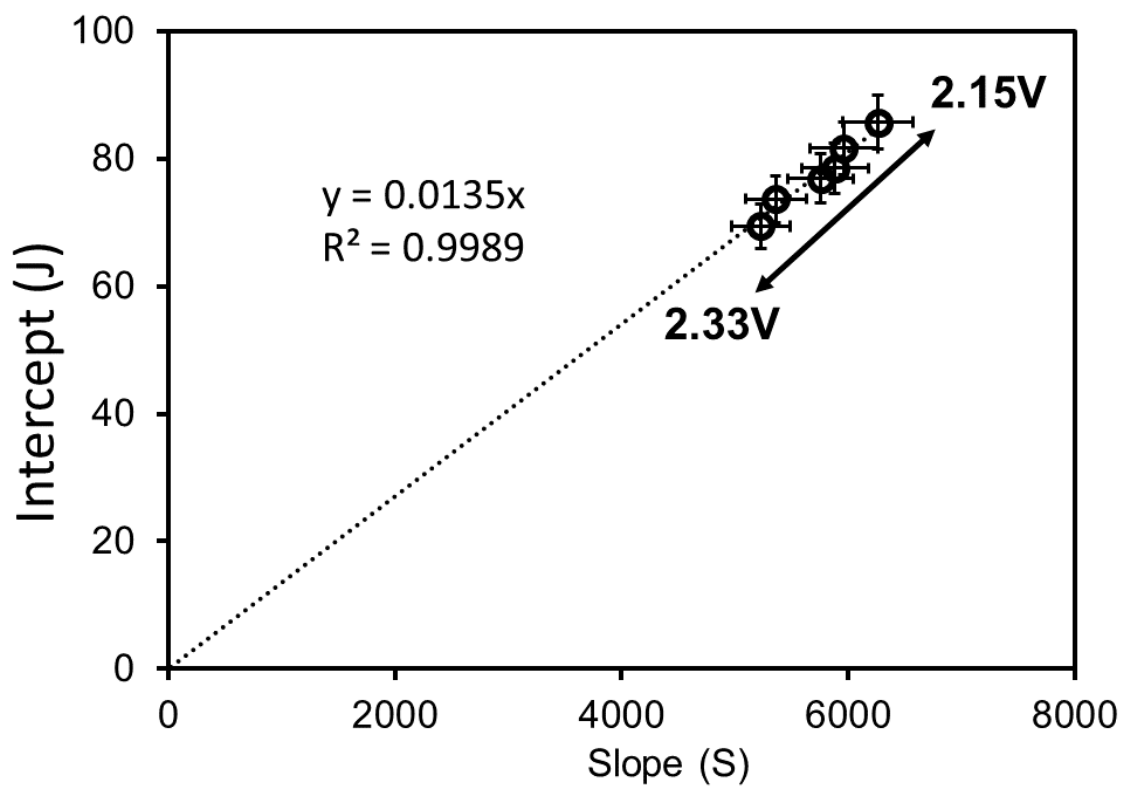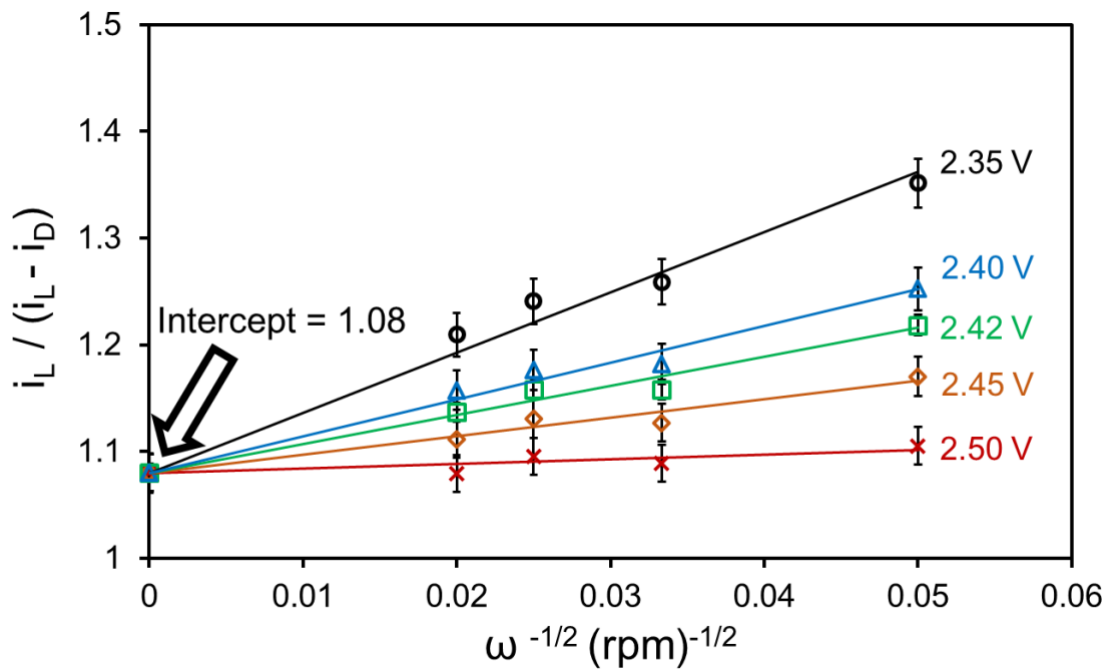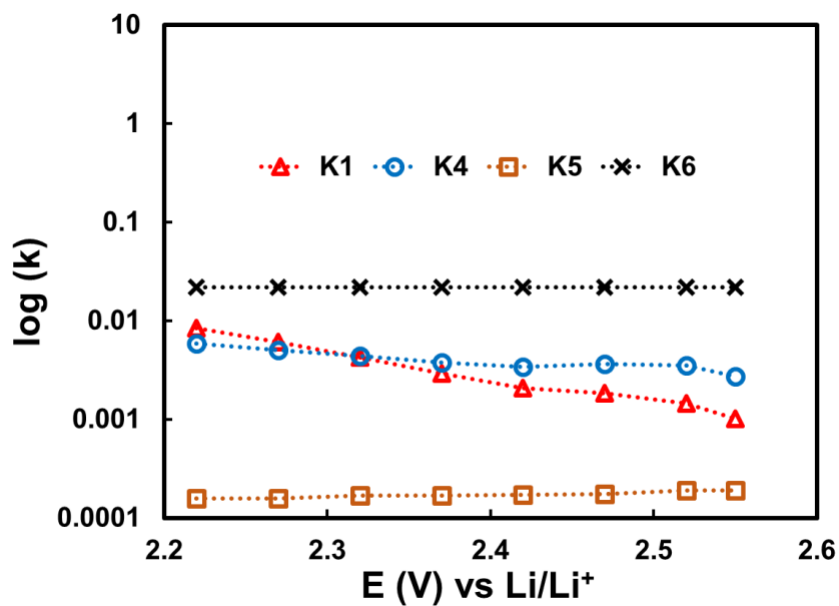
Figure 7. Slope(S) and intercept (J) plot from $N(i_D/i_R)$ vs $\omega^{-1/2}$ plots for ORR on a 1mm carbon black film (10% PTFE) deposited on a $0.196cm^2$, roughened glassy carbon (GC) disk electrode in 0.1M LiTFSI/DME electrolyte.

Figure 8. $i_L/(i_L-i_D)$ vs. $\omega^{-1/2}$ plots at different potentials for ORR on a 1mm carbon black film (10% PTFE) deposited on a 0.196cm^2, roughened glassy carbon (GC) disk electrode in 0.1M LiTFSI/DME electrolyte. Error bars depict 10% standard error.
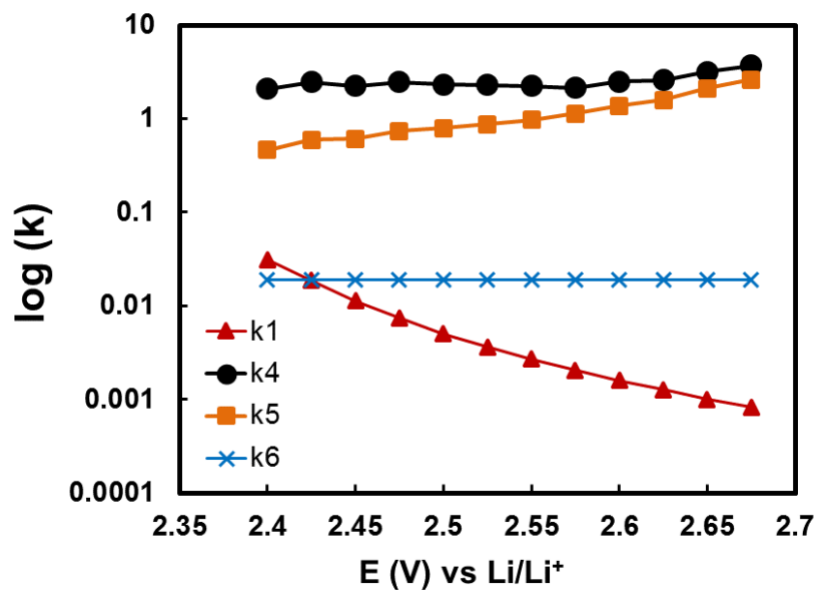
(a)

(b)

Figure 9. Calculated rate constants on **(a)** 1mm carbon black film (10% PTFE) deposited on a 0.196cm^2, roughened glassy carbon (GC); **(b)** smooth, planar glassy carbon. Data for (b) is taken from Sankarasubramanian et al. [22].

Supporting Information

Effect of cathode porosity on the Lithium air cell oxygen reduction reaction – a rotating ring-disk electrode investigation

Jeongwook Seo[a,*,#] Shrihari Sankarasubramanian[a,*,#,**], Nikhilendra Singh[b], Fuminori

Mizuno[b,c], Kensuke Takechi[b], and Jai Prakash[a,*]

*a Center for Electrochemical Science and Engineering, Department of Chemical and
Biological Engineering, Illinois Institute of Technology, 10 West 33rd Street, Chicago, IL 60616,
USA*

*b Toyota Research Institute of North America, 1555 Woodridge Avenue, Ann Arbor, Michigan
48105, USA*

Table of contents:

1.   Calibration of the Pt pseudo-reference electrode

* To whom correspondence may be addressed: E-mail address: jseo16@hawk.iit.edu (J.Seo),
ssanka11@hawk.iit.edu (S, Sankarasubramanian), prakash@iit.edu (J.Prakash)

# These authors contributed equally to this work.

c Present address: Battery Material Engineering & Research Division, Toyota Motor Corporation, Higashifuji
Technical Center, 1200, Mishuku, Susono, Shizuoka, 410-1193 Japan

** Present address: Department of Energy, Environmental and Chemical Engineering, Washington University in
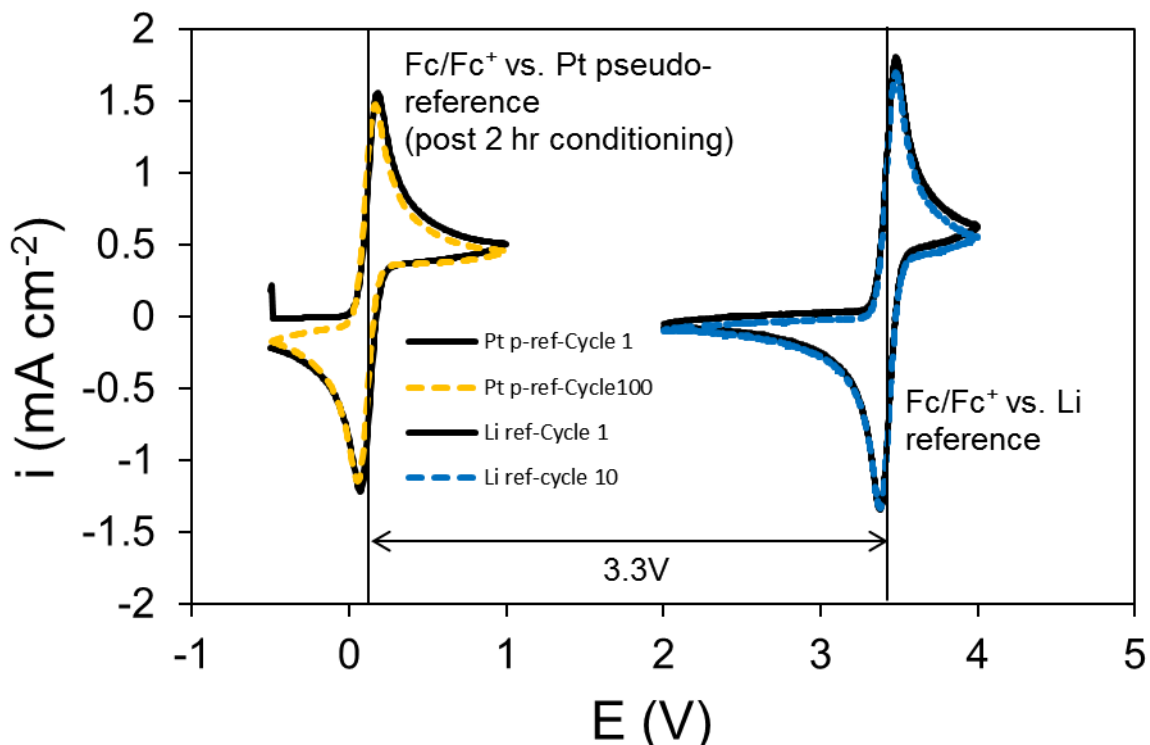St. Louis, 1 Brookings Dr, St. Louis, MO 63130, USA

Figure S1. Calibration of the Pt pseudo-reference electrode against the Li/Li$^+$ reference electrode using the ferrocene/ferrocenium (Fc/Fc$^+$) couple as an internal standard. The electrolyte was 0.5M LiTFSI in DME with 10mM ferrocene added. Scan rate = 50mV.s^{-1}.

The Pt pseudo-reference was calibrated using the ferrocene/ferrocenium internal reference as recommended by IUPAC [1]. 0.5M LiTFSI in DME was prepared in an Ar-filled glovebox(H$_2$O and O$_2$ <0.5ppm) and 10mM ferrocene added to it. The cyclic voltammograms were measured in a 3-electrode setup with a glassy carbon working electrode, a fritted Pt spiral counter electrode, with a Li metal reference, and subsequently a Pt mesh pseudo-reference. Multiple consequtive cycles were carried out to establish repreoducibility and to characterize potential drift (if any). The results are shown in Figure S1. As is evident, the Pt pseudoreference is stable within the time scale of our experiments and is seen to be suitable as a reference electrode.

References:

1. Gritzner G.; Kuta J.; Recommendations on reporting electrode potentials in nonaqueous solvents. *Pure & Appl. Chem.,* **1984,** *56 (4),* 461-466.